

# ON A QUANTITATIVE PARTIAL IMAGING PROBLEM IN VECTOR TOMOGRAPHY

HIROSHI FUJIWARA, KAMRAN SADIQ, AND ALEXANDRU TAMASAN

**ABSTRACT.** In two dimensions, we consider the problem of reconstructing a vector field from partial knowledge of its zeroth and first moment ray transforms. Different from existing works the data is known on a subset of lines, namely the ones intersecting a given arc. The problem is non-local and, for partial data, severely ill-posed. We present a reconstruction method which recovers the vector field in the convex hull of the arc. An algorithm based on this method is implemented on some numerical experiments. While still ill-posed the discretization stabilizes the numerical reconstruction.

## 1. INTRODUCTION

We consider a problem of vector tomography in the Euclidean plane where a real valued compactly supported vector field  $f = (f_1, f_2)$  is to be recovered from knowledge of its zeroth (Doppler) and first moment ray transforms

$$(1) \quad I^k f(x, \theta) := \int_{-\infty}^{\infty} t^k \theta \cdot f(\Pi_\theta(x) + t\theta) dt, \quad (x, \theta) \in \mathbb{R}^2 \times S^1, \quad k = 0, 1,$$

where  $\Pi_\theta(x) = x - (x \cdot \theta)\theta$  is the projection of  $x$  onto  $\theta^\perp$ .

In Doppler tomography [34, 31], only the zeroth moment ray transform is assumed known. Even if  $I^0 f$  is known on the manifold of all lines, it is well understood that at most one can recover the solenoidal part of the vector field. This is true for symmetric tensors of arbitrary order, where extensive work has been done for solenoidal inversion, see, e.g., [32, 27, 11, 19, 22, 23, 24] and references therein.

However, if both  $I^0 f$  and  $I^1 f$  are given on the manifold of all lines, then the entire vector field is uniquely and stably determined as shown for arbitrary order tensors in [32, 33, 2], with inversion formulas in [3, 25, 4, 14], and reconstruction methods proposed in [20, 6, 5].

For even dimensional domains the problem is non-local, where the determination of  $f$  from partial knowledge of  $(I^0 f, I^1 f)$  on a strict sub-manifold of lines becomes a question of unique analytic continuation [12]. Reconstruction methods in problems where uniqueness is based on a unique analytic continuation argument are known to be exponentially ill-posed [21].

Let  $\Omega \subset \mathbb{R}^2$  be a convex domain containing the support of  $f$  and  $\Lambda$  be a smooth arc of its boundary.

In here we consider a partial reconstruction problem in which  $f$  is to be determined on the convex hull  $\Omega^+ = \text{Conv}(\Lambda)$  from knowledge of  $I^0 f, I^1 f$  on the set  $\mathcal{S}$  of lines intersecting the arc  $\Lambda$ . More precisely,  $x$  in (1) is restricted to  $\Lambda$ . The reconstruction of  $f$  on the subdomain  $\Omega^+$  becomes a polynomially ill-posed problem. The proposed algorithm preserves this mildly ill-posedness by virtue of the choice of discretization, and thus achieves numerically stable reconstruction. We know of no other quantitative imaging method to recover  $f$  on  $\Omega^+$  from this partial data.

This novel method relies on the extension of the original theory of  $A$ -analytic maps [1] to a system of Bukhgeim-Beltrami equations as in [6] and solves a Cauchy problem with partial boundary data as in [8]. Our method requires a smooth  $f \in C_0^{1,\mu}(\Omega; \mathbb{R}^2)$ ,  $1/2 < \mu < 1$ , see Remark 1.

The partial reconstruction method is introduced in Section 2. In Section 3 we formulate a numerical algorithm and discuss the numerical stability due to the discretization. We implement the algorithm in two numerical experiments in Section 4, while in Section 5 we discuss the numerical feasibility of the method.

---

*Date:* June 23, 2025.

*2010 Mathematics Subject Classification.* Primary 65N21; Secondary 45E05.

*Key words and phrases.* Vector tomography, momenta ray transform, source reconstruction, numerical solution to Cauchy type singular integral equations,  $A$ -analytic maps, Bukhgeim-Beltrami equation, Doppler tomography.

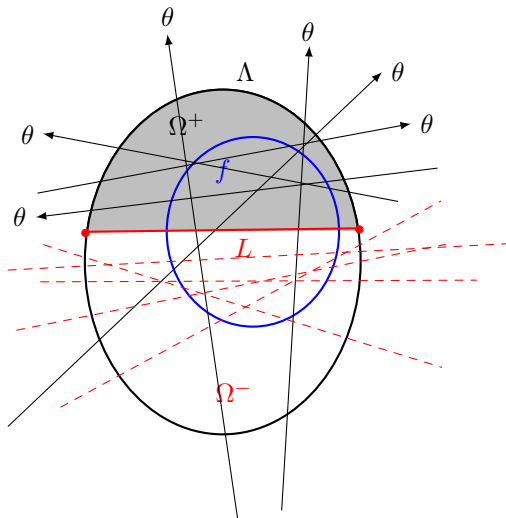


FIGURE 1.  $(I^0 f, I^1 f)$  is known on the solid lines but not on the dashed lines.

## 2. PARTIAL INVERSION OF THE MOMENTA DOPPLER TRANSFORM

The reconstruction problem is formulated as an inverse boundary value problem for a coupled system of transport equations as in [6]. We will show that the trace on  $\Lambda$  of the solution of this system uniquely determines the trace on the inner chord  $L$  (inaccessible by direct measurement), thus reducing the problem to an inverse boundary value problem with data on the entire boundary of  $\Omega^+ = \text{Conv}(\Lambda)$ .

Upon a rotation and translation of the domain, we may assume that the chord  $L$  joining the endpoints of  $\Lambda$  is the interval  $(-s, s)$  on the real axis for some  $s > 0$ , and that  $\Lambda$  lies in the upper half plane; see Figure 1 for the geometric setting.

For  $k = 0, 1$ , let  $v^k(x, \theta)$  be the unique solution to the system of transport equations:

$$(2a) \quad \theta \cdot \nabla v^0(x, \theta) = \theta \cdot f(x),$$

$$(2b) \quad \theta \cdot \nabla v^1(x, \theta) = v^0(x, \theta), \quad \text{for } (x, \theta) \in \Omega \times S^1,$$

subject to no incoming fluxes

$$(2c) \quad v^k(x, \theta) = 0, \quad \text{on } \Sigma_-,$$

where  $\Sigma_- := \{(\zeta, \theta) \in \partial\Omega \times S^1; \nu(\zeta) \cdot \theta < 0\}$  with  $\nu$  being the outer unit normal field at the boundary.

The outgoing fluxes are given only on

$$\Sigma_+ := \{(\zeta, \theta) \in \Lambda \times S^1; \nu(\zeta) \cdot \theta > 0\}.$$

The traces on  $\Sigma_+$  of the solution of the boundary value problem (2) are in a one-to-one correspondence with the momenta Doppler transform  $\langle I^0 f, I^1 f \rangle$  via the relations

$$(3) \quad \begin{aligned} v^0|_{\Sigma_+}(\zeta, \theta) &= I^0 f|_{\Sigma_+}(\zeta, \theta), \\ v^1|_{\Sigma_+}(\zeta, \theta) &= (\zeta \cdot \theta)v^0|_{\Sigma_+}(\zeta, \theta) - I^1 f|_{\Sigma_+}(\zeta, \theta), \end{aligned}$$

see [6, Proposition 2.1.].

The traces  $v^k|_{\Lambda \times S^1}$  are determined by the data via

$$(4) \quad g^0(\zeta, \theta) = \begin{cases} I^0 f(\zeta, \theta), & (\zeta, \theta) \in \Sigma_+, \\ 0, & \text{otherwise} \end{cases} \quad \text{and} \quad g^1(\zeta, \theta) = \begin{cases} (\zeta \cdot \theta)I^0 f(\zeta, \theta) - I^1 f(\zeta, \theta), & (\zeta, \theta) \in \Sigma_+, \\ 0, & \text{otherwise.} \end{cases}$$

We work with the sequence of the Fourier coefficients of  $v^k(z, \cdot)$  in the angular variable  $\theta = (\cos \varphi, \sin \varphi)$ ,

$$(5) \quad v_n^k(z) = \frac{1}{2\pi} \int_{-\pi}^{\pi} v^k(z, \theta) e^{-in\varphi} d\varphi, \quad k = 0, 1, n \in \mathbb{Z}.$$

The upper index  $k$  denotes the level of the flux, while the lower index  $n$  is the Fourier coefficient in the angular variable.

In terms of the Cauchy Riemann operators  $\partial = (\partial_x - i\partial_y)/2$  and  $\bar{\partial} = (\partial_x + i\partial_y)/2$ , the advection operator becomes  $\theta \cdot \nabla_z = e^{-i\varphi} \bar{\partial} + e^{i\varphi} \partial$ . By identifying the Fourier coefficients in (2), the solution  $v_n^k$ 's solve

$$(6a) \quad \bar{\partial} v_0^0(z) + \partial v_{-2}^0(z) = \frac{1}{2}(f_1(z) + if_2(z)),$$

$$(6b) \quad \bar{\partial} v_{-n}^0(z) + \partial v_{-n-2}^0(z) = 0, \quad n \geq 1,$$

$$(6c) \quad \bar{\partial} v_{-n}^1(z) + \partial v_{-n-2}^1(z) = v_{-n-1}^0(z), \quad n \in \mathbb{Z},$$

subject to

$$(6d) \quad v_{-n}^k|_{\Lambda} = g_{-n}^k, \quad \text{for } k = 0, 1,$$

Since the vector field  $f = \langle f_1, f_2 \rangle$  is real valued, the solution  $v^k$  of the boundary value problem (2) is also real valued, and its Fourier modes  $v_{-n}^k$  occur in conjugates,

$$(7) \quad v_n^k = \overline{v_{-n}^k}, \quad \text{for } n \geq 0, k = 0, 1.$$

Thus, it suffices to consider the non-positive Fourier modes of  $v^k(z, \cdot)$ . For  $k = 0, 1$ , let

$$\mathbf{v}^k := \langle v_0^k, v_{-1}^k, v_{-2}^k, \dots \rangle$$

be the sequence valued map of the non-positive Fourier coefficients of the solution  $v^k$  and

$$\mathbf{g}^k := \mathbf{v}^k|_{\Lambda} = \langle g_0^k, g_{-1}^k, g_{-2}^k, \dots \rangle$$

be its corresponding trace on the boundary.

In the sequence valued map notation the boundary value problem (6) becomes

$$(8a) \quad \bar{\partial} v_0^0 + \partial v_{-2}^0 = \frac{1}{2}(f_1 + if_2),$$

$$(8b) \quad \bar{\partial}[\mathcal{L}\mathbf{v}^0] + \mathcal{L}^2 \partial[\mathcal{L}\mathbf{v}^0] = \mathbf{0},$$

$$(8c) \quad \bar{\partial} \mathbf{v}^1 + \mathcal{L}^2 \partial \mathbf{v}^1 = \mathcal{L} \mathbf{v}^0,$$

subject to

$$(8d) \quad \mathbf{v}^k|_{\Lambda} = \mathbf{g}^k, \quad \text{for } k = 0, 1,$$

where  $\mathcal{L}$  denotes the left translation operator  $\mathcal{L}\mathbf{v} = \mathcal{L}(v_0, v_{-1}, v_{-2}, \dots) := (v_{-1}, v_{-2}, \dots)$ .

The system of Bukhgeim-Beltrami equations (8) are of type

$$(9) \quad \bar{\partial} \mathbf{v} + \mathcal{L}^2 \partial \mathbf{v} = \mathbf{w},$$

and solution of such a system can be expressed in terms of two operators defined component-wise for  $n \geq 0$  by

$$(10) \quad (\mathcal{B}\mathbf{v})_{-n}(z) := \frac{1}{2\pi i} \int_{\partial\Omega} \frac{v_{-n}(\zeta)}{\zeta - z} d\zeta + \frac{1}{2\pi i} \sum_{j=1}^{\infty} \int_{\partial\Omega} \left\{ \frac{d\zeta}{\zeta - z} - \frac{d\bar{\zeta}}{\bar{\zeta} - \bar{z}} \right\} v_{-n-2j}(\zeta) \left( \frac{\bar{\zeta} - \bar{z}}{\zeta - z} \right)^j,$$

$$(11) \quad (\mathcal{T}\mathbf{w})_{-n}(z) := -\frac{1}{\pi} \sum_{j=0}^{\infty} \int_{\Omega} w_{-n-2j}(\zeta) \frac{1}{\zeta - z} \left( \frac{\bar{\zeta} - \bar{z}}{\zeta - z} \right)^j d\xi d\eta, \quad \zeta = \xi + i\eta, \quad z \in \Omega,$$

see details in [28, Theorem 3.1], [6, Proposition B.1].

Solution of (9) satisfy an Abel-type result.

**Proposition 1.** *Let  $\Omega$  be a bounded convex domain,  $\mathcal{B}$  and  $\mathcal{T}$  be the operators in (10), respectively, (11), and  $\mathbf{w} \in C(\overline{\Omega}; l^1)$ . If  $\mathbf{v} \in C^1(\Omega; l^1) \cap C(\overline{\Omega}; l^1)$  solves (9). Then  $\mathcal{B}[\mathbf{v}|_r] \in C(\overline{\Omega}; l_\infty)$ ,  $\mathcal{T}\mathbf{w} \in C(\overline{\Omega}; l_\infty)$ , and*

$$(12) \quad \mathbf{v}(z) = \mathcal{B}[\mathbf{v}|_r](z) + (\mathcal{T}\mathbf{w})(z),$$

holds component-wise for every  $z \in \Omega$ . Moreover, for each  $n \geq 0$ :

$$(13) \quad \begin{aligned} \lim_{\Omega \ni z \rightarrow z_0 \in \partial\Omega} v_{-n}(z) &= \frac{1}{2\pi i} \int_{\partial\Omega} \frac{v_{-n}(\zeta)}{\zeta - z_0} d\zeta + \frac{1}{2} v_{-n}(z_0) \\ &+ \frac{1}{2\pi i} \sum_{j=1}^{\infty} \int_{\partial\Omega} \left\{ \frac{d\zeta}{\zeta - z_0} - \frac{d\bar{\zeta}}{\bar{\zeta} - \bar{z}_0} \right\} v_{-n-2j}(\zeta) \left( \frac{\bar{\zeta} - \bar{z}_0}{\zeta - z_0} \right)^j \\ &- \frac{1}{\pi} \sum_{j=0}^{\infty} \iint_{\Omega} \frac{w_{-n-2j}(\zeta)}{\zeta - z_0} \left( \frac{\bar{\zeta} - \bar{z}_0}{\zeta - z_0} \right)^j d\xi d\eta, \quad \zeta = \xi + i\eta. \end{aligned}$$

*Proof.* The regularity of  $\mathcal{B}[\mathbf{v}|_r]$  follows directly from its definition (10), as shown in [28, Theorem 3.1].

The formula (12) is shown in [6, Proposition B.1.]. The fact that

$$\lim_{\Omega \ni z \rightarrow z_0 \in \partial\Omega} \mathcal{B}[\mathbf{v}|_r](z) = \mathcal{B}[\mathbf{v}|_r](z_0) + \frac{1}{2} \mathbf{v}(z_0)$$

follows from the Sokhotski-Plemelj formula (e.g [26]) and [28, Proposition 2.2].

To justify the continuity upto the boundary of  $\mathcal{T}\mathbf{w}$ , we work in polar coordinates. Let  $\zeta(z, \varphi) = z + \rho e^{i\varphi}$ ,  $0 \leq \varphi \leq 2\pi$  and  $0 \leq \rho \leq L(z, \varphi)$ , where  $L(z, \varphi)$  is the length of the ray emanating from  $z$  in the direction  $\varphi$ , then

$$(14) \quad (\mathcal{T}\mathbf{w})_{-n}(z) = -\frac{1}{\pi} \sum_{j=0}^{\infty} \int_0^{2\pi} \int_0^{L(z, \varphi)} w_{-n-2j}(z + \rho e^{i\varphi}) e^{-i(2j+1)\varphi} d\rho d\varphi.$$

Since  $L(z, \varphi)$  is uniformly continuous in  $\overline{\Omega} \times [0, 2\pi]$  as shown in [28, Proposition 2.2] and  $\mathbf{w} \in C(\overline{\Omega}; l^1)$ , the regularity of  $\mathcal{T}\mathbf{w} \in C(\overline{\Omega}; l_\infty)$  follows. Moreover, for each  $n \geq 0$ ,

$$\lim_{\Omega \ni z \rightarrow z_0 \in \partial\Omega} (\mathcal{T}\mathbf{w})_{-n}(z) = (\mathcal{T}\mathbf{w})_{-n}(z_0).$$

□

We next show the unique determination of traces of solution  $\mathbf{v}$  of (9) from the arc  $\Lambda$  to the inner chord  $L$ . The result is a generalization of [8, Theorem 3.1].

Given the sequences  $\mathbf{v}|_\Lambda$  and  $\mathbf{w}|_{\Omega^+}$ , let us define for each  $n \geq 0$ , the functions  $F[\mathbf{v}|_\Lambda, \mathbf{w}]_{-n}$  on  $L$  except at the endpoints, by

$$(15) \quad \begin{aligned} F[\mathbf{v}|_\Lambda, \mathbf{w}]_{-n}(z) &:= \frac{1}{i\pi} \int_\Lambda \frac{v_{-n}(\zeta)}{\zeta - z} d\zeta + \frac{1}{i\pi} \sum_{j=1}^{\infty} \int_\Lambda \left\{ \frac{d\zeta}{\zeta - z} - \frac{d\bar{\zeta}}{\bar{\zeta} - z} \right\} v_{-n-2j}(\zeta) \left( \frac{\bar{\zeta} - z}{\zeta - z} \right)^j \\ &- \frac{2}{\pi} \sum_{j=0}^{\infty} \iint_{\Omega^+} \frac{w_{-n-2j}(\xi, \eta)}{(\xi - z) + i\eta} \left( \frac{(\xi - z) - i\eta}{(\xi - z) + i\eta} \right)^j d\xi d\eta, \quad z \in L. \end{aligned}$$

For the result below, let  $H_s$  denote the finite Hilbert transform of functions on  $(-s, s)$ ,

$$(16) \quad H_s[f](x) = \frac{1}{\pi} \text{p.v.} \int_{-s}^s \frac{f(y)}{x - y} dy.$$

**Proposition 2.** *Let  $\Omega \subset \mathbb{R}^2$  be a strictly convex domain,  $\Lambda$  be an arc of its boundary, and  $L$  be the chord joining the endpoints of  $\Lambda$ . Let  $\Omega^+ = \text{Conv}(\Lambda) \cap \Omega$  be the convex hull of  $\Lambda$ , and  $\mathbf{w} \in C(\overline{\Omega^+}; l^1)$  be given. If  $\mathbf{v} \in C^1(\Omega^+; l^1) \cap C(\overline{\Omega^+}; l^1)$  is the solution of (9), then its trace  $\mathbf{v}|_L$  on  $L$  is recovered pointwise from the data  $\mathbf{v}|_\Lambda$  and  $\mathbf{w}$  as follows: for each  $n \geq 0$ ,  $v_{-n}|_L$  is the unique solution in  $L^2(-s, s)$  of*

$$(17) \quad [I - iH_s](v_{-n})(x) = F[\mathbf{v}|_\Lambda, \mathbf{w}]_{-n}(x), \quad x \in L,$$

where  $F[\mathbf{v}|_\Lambda, \mathbf{w}]_{-n}$  is given by (15).

*Proof.* Since the right hand side of the non-homogeneous Bukhgeim-Beltrami (9) is known, along with its trace  $\mathbf{g} := \mathbf{v}|_\Lambda$  given, we have

$$(18a) \quad \bar{\partial}v_{-n} + \partial v_{-n-2} = w_{-n}, \quad n \geq 0,$$

$$(18b) \quad v_{-n}|_\Lambda = g_{-n}.$$

We solve (18) for  $n \geq 0$ , with partial boundary data on  $\Lambda$ , via the Bukhgeim-Pompeiu formula (12):

$$(19) \quad \begin{aligned} v_{-n}(z) := & \frac{1}{2\pi i} \int_{\partial\Omega^+} \frac{v_{-n}(\zeta)}{\zeta - z} d\zeta + \frac{1}{2\pi i} \sum_{j=1}^{\infty} \int_{\partial\Omega^+} \left\{ \frac{d\zeta}{\zeta - z} - \frac{d\bar{\zeta}}{\bar{\zeta} - \bar{z}} \right\} v_{-n-2j}(\zeta) \left( \frac{\bar{\zeta} - \bar{z}}{\zeta - z} \right)^j \\ & - \frac{1}{\pi} \sum_{j=0}^{\infty} \int_{\Omega^+} \frac{w_{-n-2j}(\zeta)}{\zeta - z} \left( \frac{\bar{\zeta} - \bar{z}}{\zeta - z} \right)^j d\xi d\eta, \quad \zeta = \xi + i\eta, \quad z \in \Omega^+. \end{aligned}$$

However, for the boundary condition (18b) to be satisfied the following compatibility condition needs to hold: By taking the non-tangential limit  $\Omega^+ \ni z \rightarrow z_0 \in \partial\Omega^+$  in (19) and using Proposition 1 yields that the trace must satisfy

$$(20) \quad \begin{aligned} v_{-n}(z_0) := & \frac{1}{2\pi i} \int_{\partial\Omega^+} \frac{v_{-n}(\zeta)}{\zeta - z_0} d\zeta + \frac{1}{2} v_{-n}(z_0) + \frac{1}{2\pi i} \sum_{j=1}^{\infty} \int_{\partial\Omega^+} \left\{ \frac{d\zeta}{\zeta - z_0} - \frac{d\bar{\zeta}}{\bar{\zeta} - \bar{z}_0} \right\} v_{-n-2j}(\zeta) \left( \frac{\bar{\zeta} - \bar{z}_0}{\zeta - z_0} \right)^j \\ & - \frac{1}{\pi} \sum_{j=0}^{\infty} \iint_{\Omega^+} \frac{w_{-n-2j}(\zeta)}{\zeta - z_0} \left( \frac{\bar{\zeta} - \bar{z}_0}{\zeta - z_0} \right)^j d\xi d\eta, \quad \zeta = \xi + i\eta, \quad z_0 \in \partial\Omega^+. \end{aligned}$$

In our inverse problem this compatibility condition is already satisfied for  $z_0 \in \Lambda$ . We use this compatibility condition for  $z_0 \in L$ , to recover the missing boundary data  $v_{-n}|_L$ . More precisely, we get

$$\begin{aligned} [I - iH_s]v_{-n}(z_0) = & \frac{1}{\pi i} \sum_{j=1}^{\infty} \int_L \left\{ \frac{d\zeta}{\zeta - z_0} - \frac{d\bar{\zeta}}{\bar{\zeta} - \bar{z}_0} \right\} v_{-n-2j}(\zeta) \left( \frac{\bar{\zeta} - \bar{z}_0}{\zeta - z_0} \right)^j \\ & + \frac{1}{\pi i} \int_\Lambda \frac{v_{-n}(\zeta)}{\zeta - z_0} d\zeta + \frac{1}{\pi i} \sum_{j=1}^{\infty} \int_\Lambda \left\{ \frac{d\zeta}{\zeta - z_0} - \frac{d\bar{\zeta}}{\bar{\zeta} - \bar{z}_0} \right\} v_{-n-2j}(\zeta) \left( \frac{\bar{\zeta} - \bar{z}_0}{\zeta - z_0} \right)^j \\ & - \frac{2}{\pi} \sum_{j=0}^{\infty} \iint_{\Omega^+} \frac{w_{-n-2j}(\xi, \eta)}{(\xi - z_0) + i\eta} \left( \frac{(\xi - z_0) - i\eta}{(\xi - z_0) + i\eta} \right)^j d\xi d\eta, \quad z_0 \in L, \end{aligned}$$

where  $H_s$  is the finite Hilbert transform in (16). Since the first integral ranges over the reals, it vanishes, and  $v_{-n}$  solves (17).

The equation (17) has a unique solution since  $i$  is not in the point spectrum of  $H_s$  (e.g., [17, 36]), thus allowing one to invert  $[I - iH_s]$  in its range.  $\square$

**2.1. Reconstruction method.** Given the data  $\langle I^0 f, I^1 f \rangle$  on lines intersecting  $\Lambda$ , we use (8d) to first determine  $\mathbf{v}^0|_\Lambda, \mathbf{v}^1|_\Lambda$  on  $\Lambda$ .

- **The recovery of the sequence  $\mathcal{L}\mathbf{v}^0$ .**

From  $\mathbf{v}^0|_\Lambda$  we compute via (15) the function  $F[\mathbf{v}^0|_\Lambda, \mathbf{0}]_{-n}$  for each  $n \geq 1$ .

For each  $n \geq 1$ , we recover the trace  $v_{-n}^0|_L$  as the unique solution of

$$(21) \quad [I - iH_s](v_{-n}^0)(x) = F[\mathbf{v}^0|_\Lambda, \mathbf{0}]_{-n}(x), \quad x \in L.$$

By using the Bukhgeim-Cauchy formula (10), we extend  $\mathcal{L}\mathbf{v}^0$  from  $\Lambda \cup L$  to  $\Omega^+$ :

$$(22) \quad \mathcal{L}\mathbf{v}^0 := \mathcal{B}(\mathcal{L}\mathbf{v}^0|_{\Lambda \cup L}), \quad \text{in } \Omega^+.$$

Thus,  $v_{-n}^0$  for  $n \geq 1$  is recovered inside  $\Omega^+$ . Note that the mode  $v_0^0$  is not yet determined.

- **The recovery of the entire sequence  $\mathbf{v}^1$ .**

From data  $\mathbf{v}^1|_\Lambda$  and  $\mathcal{L}\mathbf{v}^0$  in (22), we use (15) to compute  $F[\mathbf{v}^1|_\Lambda, \mathcal{L}\mathbf{v}^0]_{-n}$  for each  $n \geq 0$ .

For each  $n \geq 0$ , the trace  $v_{-n}^1|_L$  is recovered as the unique solution of

$$(23) \quad [I - iH_s](v_{-n}^1)(x) = F[\mathbf{v}^1|_\Lambda, \mathcal{L}\mathbf{v}^0]_{-n}(x), \quad x \in L.$$

Next, we determine the entire sequence  $\mathbf{v}^1$  in  $\Omega^+$  by using the Bukhgeim-Pompeiu formula (12):

$$(24) \quad \mathbf{v}^1 := \mathcal{B}(\mathbf{v}^1|_{\Lambda \cup L}) + \mathcal{T}(\mathcal{L}\mathbf{v}^0), \quad \text{in } \Omega^+.$$

- **The reconstruction of the Fourier mode  $v_0^0$ .**

The real valued mode  $v_0^0$  is determined via (6c) for  $n = 1$ , and the complex conjugate relation (7),

$$(25) \quad v_0^0(z) := \bar{\partial}v_1^1(z) + \partial v_{-1}^1(z) = 2 \operatorname{Re} \partial v_{-1}^1(z), \quad z \in \Omega^+.$$

Note that (22) and (25) now yield the entire sequence  $\mathbf{v}^0$  in  $\Omega^+$ .

- **The recovery of the vector field.**

From the mode  $v_{-2}^0$  in (22) and the mode  $v_0^0$  in (25) we recover the vector field inside by

$$(26) \quad f(z) := \langle 2 \operatorname{Re} \{ \bar{\partial}v_0^0(z) + \partial v_{-2}^0(z) \}, 2 \operatorname{Im} \{ \bar{\partial}v_0^0(z) + \partial v_{-2}^0(z) \} \rangle, \quad z \in \Omega^+.$$

□

**Remark 1.** *The occurring series in the reconstruction method requires justification for their convergence. This follows from the assumed regularity of the vector field  $f$ . More precisely, since  $f$  is assumed in  $C_0^{1,\mu}(\Omega; \mathbb{R}^2)$ ,  $1/2 < \mu < 1$ , the solution  $v^k$  of system (2) lies in  $C^{1,\mu}(\bar{\Omega} \times \mathbb{S}^1)$ . In particular, the traces  $v^k|_{\Lambda \times \mathbb{S}^1} \in C^{1,\mu}(\Lambda; C^{1,\mu}(\mathbb{S}^1))$  and [28, Proposition 4.1 (i)] applies to yield the regularity in the sequence valued data  $\mathbf{g}^k \in l_\infty^{1,1}(\Lambda) \cap C^{1,\mu}(\Lambda; l_1)$ , for  $k = 0, 1$ . We refer to [28] for the definition of the spaces. This induced regularity in the data suffices for the equations (21) - (26) in the reconstruction method to make sense, and have a unique solution.*

### 3. RECONSTRUCTION ALGORITHM

This section presents a numerical algorithm based on the reconstruction method above.

Let  $\{\zeta(\omega); \alpha_0 < \omega < \alpha_K\}$  be a smooth parametrization of  $\Lambda$  with  $s = \zeta(\alpha_0)$  and  $-s = \zeta(\alpha_K)$ . The arc is further divided into  $K$  sub-arcs associated with the partition  $\alpha_0 < \alpha_1 < \dots < \alpha_K$ . For  $1 \leq k \leq K$ , let  $\Delta\omega_k = \alpha_k - \alpha_{k-1}$  denote the interval width. At the midpoint  $\omega_k = (\alpha_{k-1} + \alpha_k)/2$  of each interval, we write  $\zeta_k = \zeta(\omega_k)$  and  $\zeta'_k = \zeta'(\omega_k)$ . Let  $\Delta\varphi = \frac{2\pi}{N}$ ,  $\varphi_n = \left(n - \frac{1}{2}\right) \Delta\varphi$  for  $1 \leq n \leq N$ , and  $\theta_n = (\cos \varphi_n, \sin \varphi_n)$ .

The data is sampled on  $\Lambda$  with respect to the outgoing direction; more specifically, our measurement data consists of

$$\{I^0 f(\zeta_k, \theta_n); 1 \leq k \leq K, 1 \leq n \leq N, (\zeta_k, \theta_n) \in \Sigma_+\}$$

and

$$\{I^1 f(\zeta_k, \theta_n); 1 \leq k \leq K, 1 \leq n \leq N, (\zeta_k, \theta_n) \in \Sigma_+\}.$$

Let  $M$  be a positive integer to truncate the occurring Fourier series. For a positive integer  $J$ , we write  $\Delta x = \frac{2s}{J}$  and equi-spaced points on  $L = (-s, s)$  by  $x_j = -s + \left(j - \frac{1}{2}\right) \Delta x$ ,  $1 \leq j \leq J$ . Let

$$G = \begin{cases} \{G_m(\zeta_k), G_{m-2}(\zeta_k), \dots, G_{-2M}(\zeta_k); 1 \leq k \leq K\}, & \text{if } m \text{ is even,} \\ \{G_m(\zeta_k), G_{m-2}(\zeta_k), \dots, G_{-2M+1}(\zeta_k); 1 \leq k \leq K\}, & \text{if } m \text{ is odd,} \end{cases}$$

and

$$V_L = \begin{cases} \{V_m(x_j), V_{m-2}(x_j), \dots, V_{-2M}(x_j); 1 \leq j \leq J\}, & \text{if } m \text{ is even,} \\ \{V_m(x_j), V_{m-2}(x_j), \dots, V_{-2M+1}(x_j); 1 \leq j \leq J\}, & \text{if } m \text{ is odd.} \end{cases}$$

The proposed algorithms are described with operators for  $-1 \geq m \geq -2M$ :

$$\begin{aligned} \mathcal{F}_m[G](x) = & -\frac{1}{\pi i} \sum_{k=1}^K \frac{G_m(\zeta_k)}{x - \zeta_k} \zeta_k' \Delta\omega_k \\ & + \frac{2}{\pi} \sum_{k=1}^K \left\{ \sum_{m-2 \geq m-2j \geq -2M} G_{m-2j}(\zeta_k) \left( \frac{\bar{\zeta}_k - x}{\zeta_k - x} \right)^j \right\} \operatorname{Im} \left( \frac{\zeta_k'}{\zeta_k - x} \right) \Delta\omega_k, \quad x \in L, \end{aligned}$$

and the discretization of the  $\mathcal{B}$  operator in (10) for  $-1 \geq m \geq -2M$ :

$$\begin{aligned} (27) \quad \mathcal{B}_m[V_L, G](c) = & \frac{1}{2\pi i} \sum_{\ell=1}^J \frac{V_m(x_\ell)}{x_\ell - c} \Delta x + \frac{1}{2\pi i} \sum_{k=1}^K \frac{G_m(\zeta_k)}{\zeta_k - c} \zeta_k' \Delta\omega_k \\ & + \frac{1}{2\pi i} \sum_{\ell=1}^J \left\{ \sum_{m-2 \geq m-2j \geq -2M} V_{m-2j}(x_\ell) \left( \frac{x_\ell - \bar{c}}{x_\ell - c} \right)^j \right\} \left( \frac{1}{x_\ell - c} - \frac{1}{x_\ell - \bar{c}} \right) \Delta x \\ & + \frac{1}{\pi} \sum_{k=1}^K \left\{ \sum_{m-2 \geq m-2j \geq -2M} G_{m-2j}(\zeta_k) \left( \frac{\bar{\zeta}_k - \bar{c}}{\zeta_k - c} \right)^j \right\} \operatorname{Im} \left( \frac{\zeta_k'}{\zeta_k - c} \right) \Delta\omega_k, \quad c \in \Omega^+. \end{aligned}$$

**Step 1.** Introduce an inscribed polygonal domain  $\Omega_\Delta^+ \approx \Omega^+$  whose closure includes  $L$ . We also take a triangulation  $\{\tau_s; 1 \leq s \leq S\}$  of  $\Omega_\Delta^+$ , i.e. each  $\tau_s$  is a triangular domain,  $\tau_s \cap \tau_t = \emptyset$  if  $s \neq t$ , and  $\Omega_\Delta^+ = \bigcup_{1 \leq s \leq S} \tau_s$ . We denote by  $c_s = (c_{s,x}, c_{s,y})$  the centroid of the triangle  $\tau_s$ .

**Step 2.** [Preparation of regularized differentiation in Step 10 below.] For each triangle  $\tau_s$ , assign the corresponding sets of triangles  $\mathcal{N}_s$  which will be used in the numerical differentiation. For the sake of clarity, we call  $\mathcal{N}_s$  a *neighborhood* of  $\tau_s$ .

**Step 3.** [Discretization of the  $\mathcal{T}$  operator (11).] It is easy to see that the integrands in (11) have removable singularities when using polar coordinates, which yields to the computation of the integrals

$$\Psi(c; \tau) := \int_{-\pi}^{\pi} \rho_\tau(c; \varphi) e^{-(2j+1)i\varphi} d\varphi$$

for each triangle  $\tau$  and  $c \in \{c_s; 1 \leq s \leq S\} \cup \{x_j \in L; 1 \leq j \leq J\}$ . If  $c$  is inside the triangle  $\tau$ , then  $\rho_\tau(c; \varphi)$  is the distance from  $c$  to the boundary of the triangle  $\tau$  in the  $\varphi$ -direction. If  $c$  is exterior to  $\tau$ , then  $\rho_\tau$  is the length of the segment determined by the intersection of the semi-line from  $c$  in the direction of  $\varphi$ -direction with the triangle  $\tau$ ; see Fig. 2.



FIGURE 2. The length  $\rho_m(z; \varphi)$  cut by the triangle  $\tau_m$ . The case for  $z \in \tau_m$  (left) and that for  $z \notin \tau_m$  (right)

One way to estimate the  $\Psi(c; \tau)$  is by a quadrature rule with  $\rho_\tau$  calculated algebraically. The discretized version of  $\mathcal{T}$  becomes

$$\mathcal{T}_m[V_{\Omega^+, \text{even}}^0](x_j) = -\frac{1}{\pi} \sum_{s=1}^T \sum_{m-1 \geq m-2j-1 \geq -2M} V_{m-2j-1}^0(c_s) \Psi(x_j; \tau_s) \quad 1 \leq j \leq J,$$

and

$$\mathcal{T}_m[V_{\Omega^+, \text{even}}^0](c_t) = -\frac{1}{\pi} \sum_{s=1}^T \sum_{m-1 \geq m-2j-1 \geq -2M} V_{m-2j-1}^0(c_s) \Psi(c_t; \tau_s) \quad 1 \leq t \leq S,$$

where  $V_{\Omega^+, \text{even}}^0 = \{V_{m-1}^0(c_s), V_{m-3}^0(c_s), \dots, V_{-2M}^0(c_s); 1 \leq s \leq S\}$ . Note that  $\mathcal{T}_m$  always appears with the odd suffix  $m$ .

**Step 4.** [Discretization of the data  $g^0$  in (4).] Let for  $1 \leq k \leq K$  and  $1 \leq n \leq N$

$$g^0(\zeta_k, \theta_n) = \begin{cases} I^0 f(\zeta_k, \theta_n), & (\zeta_k, \theta_n) \in \Sigma_+; \\ 0, & \text{otherwise.} \end{cases}$$

Then compute for  $1 \leq k \leq K$  and  $m = -2, -4, \dots, -2M$

$$G_m^0(\zeta_k) = \frac{1}{2\pi} \sum_{n=1}^N g^0(\zeta_k, \theta_n) e^{-im\varphi_n} \Delta\varphi.$$

**Step 5.** [Discretization of the singular integral equation (21).] Find  $V_{L, \text{even}}^0 = \{V_m^0(x_j); m = -2, -4, \dots, -2M, 1 \leq j \leq J\}$  by solving the discretized version of (21):

$$(28) \quad V_m^0(x_j) - \frac{i}{\pi} \sum_{\ell \neq j} \frac{V_m^0(x_\ell)}{x_j - x_\ell} \Delta x = \mathcal{F}_m[G_{\text{even}}^0](x_j).$$

**Step 6.** [Determining the modes inside  $\Omega^+$  by discretization of the equation (22).] Compute for  $m = -2, -4, \dots, -2M$  and  $1 \leq s \leq S$

$$V_m^0(c_s) = \mathcal{B}_m[V_{L, \text{even}}^0, G_{\text{even}}^0](c_s).$$

We set  $V_{\Omega^+, \text{even}}^0 = \{V_{-2}^0(c_s), \dots, V_{-2M}^0(c_s); 1 \leq s \leq S\}$ .

**Step 7.** [Discretization of the data  $g^1$  in (4).] Let for  $1 \leq k \leq K$  and  $1 \leq n \leq N$

$$g^1(\zeta_k, \theta_n) = \begin{cases} (\zeta_k \cdot \theta_n) I^0 f(\zeta_k, \theta_n) - I^1 f(\zeta_k, \theta_n), & (\zeta_k, \theta_n) \in \Sigma_+; \\ 0, & \text{otherwise,} \end{cases}$$

Then for  $1 \leq k \leq K$  and  $m = -1, -3, \dots, -2M + 1$ , compute

$$G_m^1(\zeta_k) = \frac{1}{2\pi} \sum_{n=1}^N g^1(\zeta_k, \theta_n) e^{-im\varphi_n} \Delta\varphi.$$

We set  $G_{\text{odd}}^1 = \{G_m^1(\zeta_k); m = -1, -3, \dots, -2M + 1, 1 \leq k \leq K\}$ .

**Step 8.** [Discretization of the singular integral equation (23).] Find  $V_{L, \text{odd}}^1 = \{V_m^1(x_j); m = -1, -3, \dots, -2M + 1, 1 \leq j \leq J\}$  by solving the discretized version of (23):

$$V_m^1(x_j) - \frac{i}{\pi} \sum_{\ell \neq j} \frac{V_m^1(x_\ell)}{x_j - x_\ell} \Delta x = \mathcal{F}_m[G_{\text{odd}}^1](x_j) + 2\mathcal{T}_m[V_{\text{even}}^0](x_j).$$

**Step 9.** [Determining the modes inside  $\Omega^+$  by discretization of the equation (24).] Compute for  $1 \leq s \leq S$

$$V_{-1}^1(c_s) = \mathcal{B}_{-1}[V_{L, \text{odd}}^1, G_{\text{odd}}^1](c_s) + \mathcal{T}_{-1}[V_{\Omega^+, \text{even}}^0](c_s).$$

**Step 10.** [Numerical differentiation] Using neighborhood  $\mathcal{N}_s$ , determine  $\{\partial_x V_{-2}^0(c_s), \partial_y V_{-2}^0(c_s); 1 \leq s \leq S\}$  as the least square solution to

$$(\xi_t - \xi_s) \partial_x V_{-2}^0(c_s) + (\eta_t - \eta_s) \partial_y V_{-2}^0(c_s) = V_{-2}^0(c_t) - V_{-2}^0(c_s), \quad \text{for all } t \neq s \text{ with } \tau_t \in \mathcal{N}_s, 1 \leq t \leq S.$$

Using neighborhood  $\mathcal{N}_s$ , determine  $\{\partial_x V_{-1}^1(c_s), \partial_y V_{-1}^1(c_s), \partial_{xx}^2 V_{-1}^1(c_s), \partial_{xy}^2 V_{-1}^1(c_s), \partial_{yy}^2 V_{-1}^1(c_s); 1 \leq s \leq S\}$  as the least square solution to

$$\begin{aligned} & (\xi_t - \xi_s) \partial_x V_{-1}^1(c_s) + (\eta_t - \eta_s) \partial_y V_{-1}^1(c_s) \\ & + \frac{1}{2} \{(\xi_t - \xi_s)^2 \partial_{xx}^2 V_{-1}^1(c_s) + 2(\xi_t - \xi_s)(\eta_t - \eta_s) \partial_{xy}^2 V_{-1}^1(c_s) + (\eta_t - \eta_s)^2 \partial_{yy}^2 V_{-1}^1(c_s)\} \\ & = V_{-1}^1(c_t) - V_{-1}^1(c_s), \quad \text{for all } t \neq s \text{ with } \tau_t \in \mathcal{N}_s, 1 \leq t \leq S. \end{aligned}$$

**Step 11.** Compute for  $1 \leq s \leq S$

$$\begin{aligned} F_1(c_s) &= \frac{1}{4} \left( \partial_{xx}^2 V_{-1}^1(c_s) + \partial_{yy}^2 V_{-1}^1(c_s) \right) \\ & + \frac{1}{4} \overline{\left( \partial_{xx}^2 V_{-1}^1(c_s) - \partial_{yy}^2 V_{-1}^1(c_s) - 2i \partial_{xy}^2 V_{-1}^1(c_s) \right)} + \frac{1}{2} \left( \partial_x V_{-2}^0(c_s) - i \partial_y V_{-2}^0(c_s) \right). \end{aligned}$$

**Step 12.** [Reconstruction of  $f$  via the equation (26).] Compute for  $1 \leq s \leq S$

$$f|_{\tau_s} \approx \langle 2 \operatorname{Re} F_1(c_s), 2 \operatorname{Im} F_1(c_s) \rangle.$$

This ends the algorithm.  $\square$

In the algorithm two issues are critical: the solvability of the discretized singular integral equations in Step 5 and Step 8, and the numerical differentiation in Step 10. While inversion of  $[I - iH_s]$  is severely ill-posed (since  $-i$  is in the continuous spectrum of  $H_s$  [17, 36]), its discretized version in (28) is just mildly ill-posed, where the condition number grows linearly with respect to the number of nodes  $J$ , see [9, Theorem 3.1]. The stability and accuracy in the numerical differentiation in Step 10 are controlled by the choice of neighborhoods in  $\mathcal{N}_s$ . This choice provides a regularization for the algorithm.

In our previous studies [6, 7, 9], triangles sharing vertices or edges with  $\tau_s$  have been chosen as  $\mathcal{N}_s$  for computing the first order derivatives. However, in the method for partial data requires taking some second order derivatives, thus making the procedure more numerically unstable. To overcome it, we adopt a neighborhood consisting of all the triangles whose centers are at distance at most  $R$  from center of  $\tau_s$ :  $\mathcal{N}_s(R) = \{\tau_t; |c_t - c_s| < R\}$ . The effectiveness of this strategy is discussed in detail in the next section using numerical experiments.

**Remark 2.** *The proposed algorithm adapts to the case of data on the entire boundary (all set of lines passing through the support of  $f$ ), a problem considered by the authors in [6]. Specifically, Step 5 and Step 8 are replaced by the evaluation*

$$V_m^0(c_s) := \mathcal{B}_m [G_{\text{even}}^0](c_s),$$

while Step 6 and Step 9 are replaced by

$$V_{-1}^1(c_s) := \mathcal{B}_{-1} [G_{\text{odd}}^1](c_s) + \mathcal{T}_{-1} [V_{\Omega^+, \text{even}}^0](c_s),$$

where

$$\begin{aligned} \mathcal{B}_m [G](c) &= \frac{1}{2\pi i} \sum_{k=1}^K \frac{G_m(\zeta_k)}{\zeta_k - c} \zeta_k' \Delta\omega_k \\ & + \frac{1}{\pi} \sum_{k=1}^K \left\{ \sum_{m-2 \geq m-2j \geq -2M} G_{m-2j}(\zeta_k) \left( \frac{\bar{\zeta}_k - \bar{c}}{\zeta_k - c} \right)^j \right\} \operatorname{Im} \left( \frac{\zeta_k'}{\zeta_k - c} \right) \Delta\omega_k, \quad c \in \Omega, \end{aligned}$$

and  $\zeta_k$  are now distributed on the entire boundary.

#### 4. NUMERICAL EXPERIMENTS

In this section we apply the proposed algorithm to two numerical examples, and do a quantitative study on the numerical stability and accuracy.

In both experiments the domain  $\Omega$  is the unit disc and  $\Omega^+ = \{x^2 + y^2 < 1, y > 0\}$ . The triangulation of  $\Omega_{\Delta}^+$  consists of 853 triangles, and the average of diameters of triangles is approximately 0.0766. In Step 2, we choose the set of neighboring triangles  $\mathcal{N}_s(R)$  with distance at most 0.15 from the center of

$\tau_s$ ;  $R = 0.15$ . This choice allows us to consider the second layer of neighboring triangles to be taken into  $N_s$ . The direction  $\theta$  is discretized by  $\Delta\varphi = 2\pi/1,440$ , and the number of measurement nodes on arc  $\Lambda$  is 720. In order to avoid the inverse crime, we simulate the data by applying the Gauss-Legendre numerical quadrature with 32 points to compute the integrals

$$(29a) \quad v^0(z, \theta) = \int_0^{\theta \cdot (z - z_{\text{in}})} \theta \cdot f(z_{\text{in}} + t\theta) dt,$$

and

$$(29b) \quad v^1(z, \theta) = \int_0^{\theta \cdot (z - z_{\text{in}})} v^0(z_{\text{in}} + t\theta) dt,$$

where  $t_0 = \inf\{t \in \mathbb{R} \mid z + t\theta \in \Omega\}$  and  $z_{\text{in}} = z + t_0\theta$  with  $z \in \Lambda$ , and we do not solve the system of transport equation (2) by neither finite element methods nor finite difference methods to obtain this data.

The number of discretization of the chord  $L = (-1, 1)$  is  $J = 458$ , and thus  $\Delta x = 2/458 \approx 0.00437 \approx \pi/720$ . Throughout the section, all computations are processed on EPYC 7643 with 96 cores OpenMP parallel computation by the IEEE754 double precision arithmetic. We use  $M = 128$  to truncate the Fourier series, where the highest Fourier mode used in the reconstruction is  $-256$ .

**Experiment 1.** We consider the reconstruction of the vector field ([15], also see Fig. 3)

$$(30) \quad f(x, y) = \nabla \left( \sin \pi(x^2 + y^2) \right) + f^s(x, y),$$

where

$$(31) \quad f^s(x, y) = \begin{pmatrix} 2xy \cos(x^2 + y^2) + \cos(6xy) - 6xy \sin(6xy) \\ -\sin(x^2 + y^2) - 2x^2 \cos(x^2 + y^2) + 6y^2 \sin(6xy) \end{pmatrix}$$

is the solenoidal part of  $f$ .

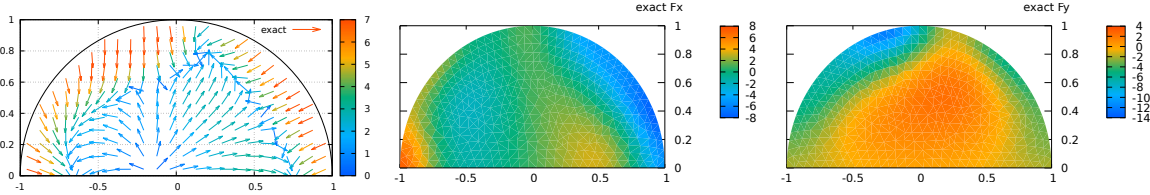


FIGURE 3. Exact vector field  $f$  in (30):  $f = \langle f_1, f_2 \rangle$  (left),  $f_1$  (middle), and  $f_2$  (right)

For  $(\zeta, \theta) \in \Sigma_+$ , the simulated data  $I^j f(\zeta, \theta)$ ,  $j = 0, 1$  in (1) are computed by numerical quadrature; see the sinograms in Fig. 4, where white areas correspond to non-observed data on  $\partial\Omega \setminus \Lambda$ .

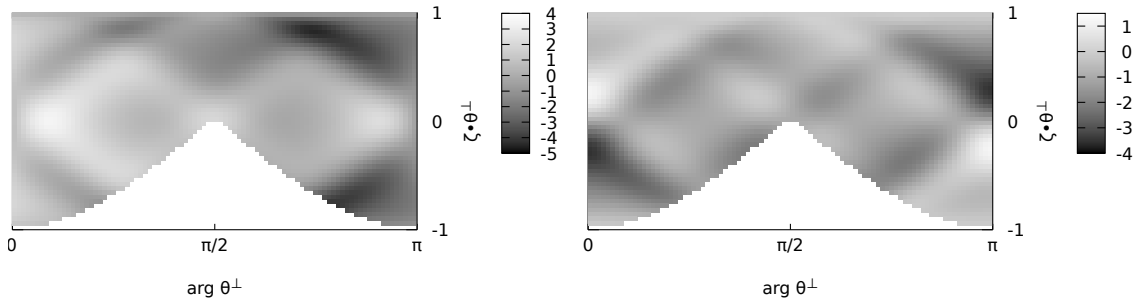


FIGURE 4. Sinogram of the noiseless simulated data  $I^0 f$  (left) and  $I^1 f$  (right) for  $f$  in (31)

Fig. 5 shows the reconstruction results via the proposed method. The reconstruction error in the  $L^2$  sense is 48.1%. Fig. 7 illustrates the reconstruction results via the proposed method from noisy data:

$I^0 f$  contains 6.0% additive noise, while  $I^1 f$  contains 4.2% additive noise. This difference in relative errors is due to the built-in pseudo-random number routine used in experiments. The reconstruction errors in the  $L^2$  sense is 48.3%. Each numerical computation for reconstruction consumes approximately 25 seconds. A detailed study of the effect of regularization via different choices of the neighborhood  $\mathcal{N}_s$  in differentiation is left for a separate discussion. Numerical results by the proposed method contains significantly larger errors compared to those in measurement data summarized in Table 1 that also include the errors in the case with whole boundary measurement.

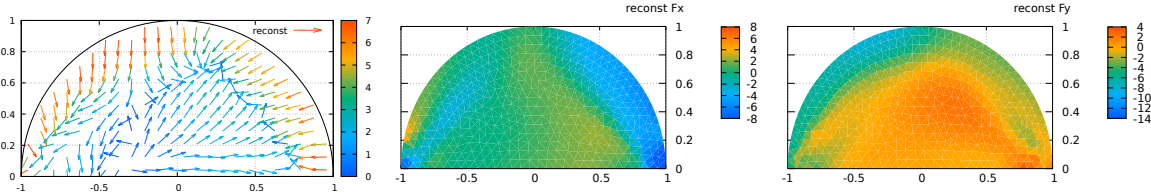


FIGURE 5. Numerical reconstruction from noiseless simulated data in Fig. 4

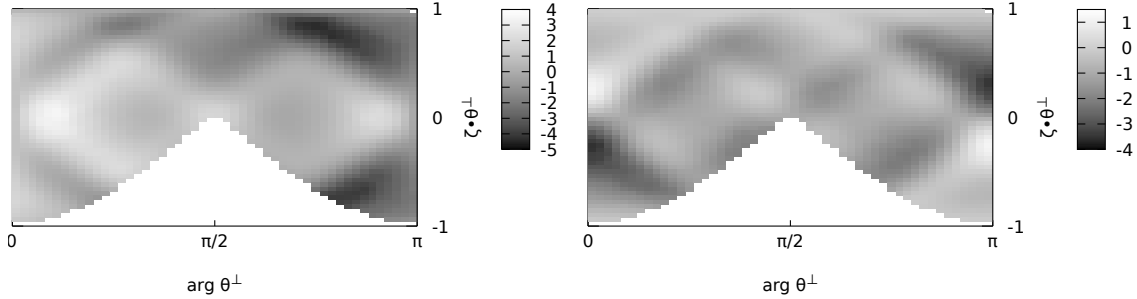


FIGURE 6. Sinogram of the noisy simulated data  $I^0 f$  (left) and  $I^1 f$  (right) for  $f$  in (31)

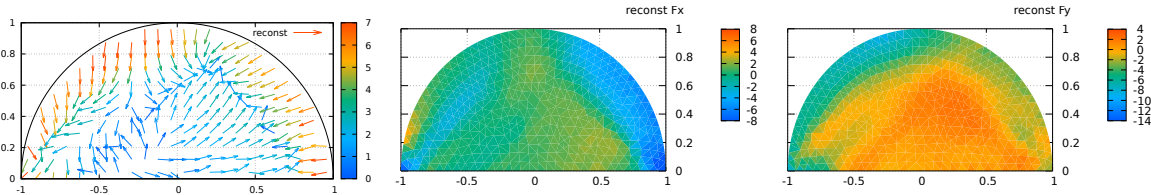


FIGURE 7. Numerical reconstruction from noisy data in Fig. 6

Aside from the inaccuracy due to the ill-posedness in differentiation, the reconstruction is less accurate near  $L$  due to the ill-posedness of the singular integral equation (21). We illustrate this lack of accuracy by comparing the error in two different regions: in the upper half domain  $\Omega_{\Delta}^{+}$ , and a subset strictly included in the upper half plane

$$\Omega_{\Delta}^{+, \text{up}} = \bigcup_{\substack{1 \leq s \leq S \\ c_{s,y} > 0.1}} \tau_s.$$

It is observed that the reconstruction near the boundary is unstable since the singular integral equation amplifies the error. We can say that concentration of errors near the boundary is expected due to theoretical evaluation of numerical integration. Although the integral is not singular, it is numerically singular near the end of the chord. This is a drawback to reconstruct near the boundary, but good for interior reconstruction.

Table 1 contrast the errors in the reconstruction using the partial data case with the full data case. The reconstruction in the partial data case is obtained by the proposed algorithm, while in the full data case we use the adapted algorithm in Remark 2. Note that magnitude of errors in  $\Omega_{\Delta}^{+}$  and  $\Omega_{\Delta}^{+,up}$  are in the same range for the full measurement case, while errors in  $\Omega_{\Delta}^{+,up}$  is remarkably smaller than those in  $\Omega_{\Delta}^{+}$  for partial measurement case. These results confirmed that errors in the proposed method for partial measurement concentrate near the chord.

TABLE 1. Errors in Experiment 1 measured in the domains  $\Omega_{\Delta}^{+}$  and  $\Omega_{\Delta}^{+,up}$ .

	full measurement		partial measurement	
	noiseless data	noisy data	noiseless data	noisy data
Noise in $I^0 f$	0%	4.8%	0%	6.0%
Noise in $I^1 f$	0%	5.6%	0%	4.2%
Error in $L^2(\Omega_{\Delta}^{+})$	14.0%	15.2%	48.1%	48.3%
Error in $L^2(\Omega_{\Delta}^{+,up})$	14.0%	15.0%	37.3%	37.8%

From Table 1, we also observe that the proposed schemes do not show significant differences in the reconstruction from noiseless vs. noisy data. This indicates that the proposed method, while not highly accurate, is stable. It also emphasizes that the numerical differentiation is one of the main factors affecting the accuracy.

**Experiment 2.** We consider the vector fields

$$(32) \quad f(x, y) = \nabla \left( \arctan \frac{y}{2+x} \right) + f^s(x, y),$$

which has the same solenoidal part (31) as Experiment 1. The vector field is depicted in Fig. 8 along with its components  $f_1$  and  $f_2$  measured on the upper semi-disc. Fig. 9 depicts the simulated

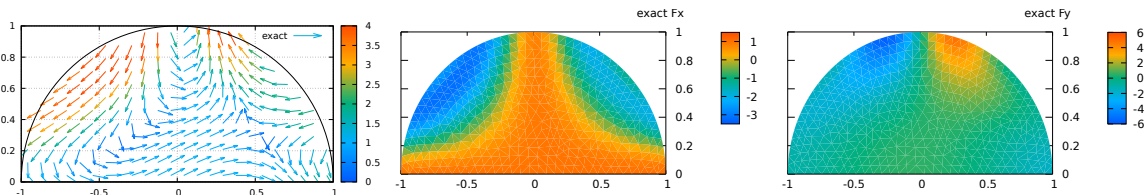


FIGURE 8. Exact vector field  $f$  in (32):  $f = \langle f_1, f_2 \rangle$  (left),  $f_1$  (middle), and  $f_2$  (right)

measurement data to this vector field as the sinograms.

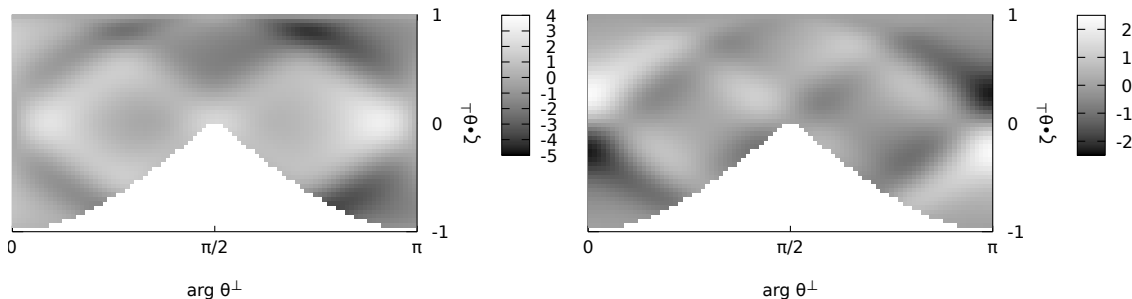


FIGURE 9. Sinogram of the noiseless simulated data  $I^0 f$  (left) and  $I^1 f$  (right) for  $f$  in (32)

To this partial measurement data, we can reconstruct the vector field in upper semi-disc shown in Fig. 10, which has 80.9% relative errors in the  $L^2$  sense with  $\mathcal{N}_s(0.15)$ . When we put 6.8% and 3.0%

measurement errors in  $I^0 f$  and  $I^1 f$  respectively illustrated in Fig. 11, we can obtain results shown in Fig. 12, which has 77.4% errors. Table 2 contrast the errors in the reconstruction using the partial data case with the full data case, and they show similar trends as in Experiment 1.

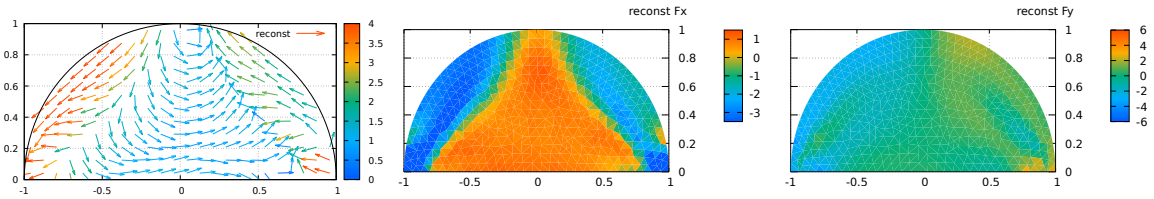


FIGURE 10. Numerical reconstruction from noiseless simulated data in Fig. 8

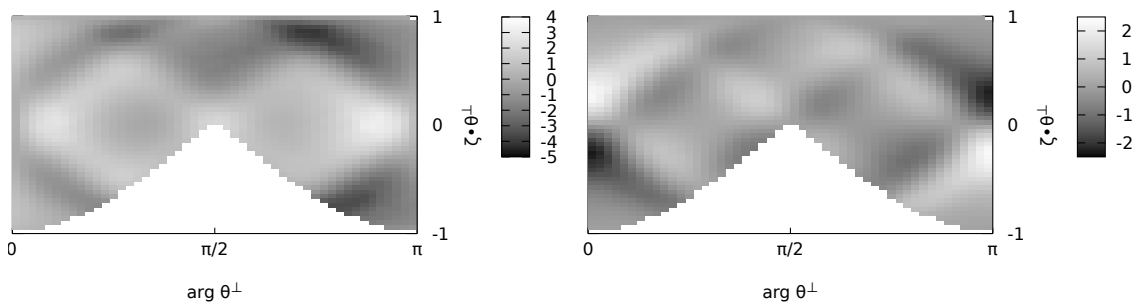


FIGURE 11. Sinogram of the noisy simulated data  $I^0 f$  (left) and  $I^1 f$  (right) for  $f$  in (32)

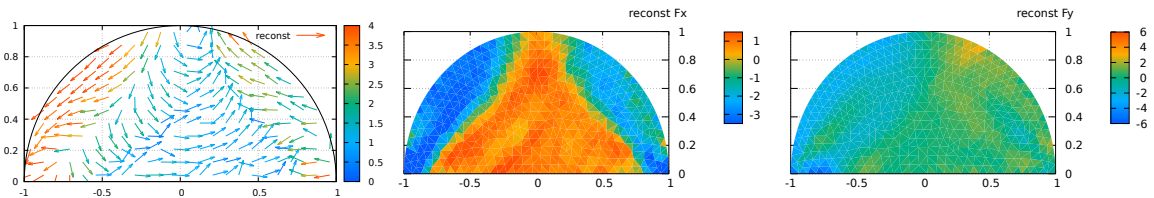


FIGURE 12. Numerical reconstruction from noisy data in Fig. 11

TABLE 2. Errors in Experiment 2 measured in the domains  $\Omega_{\Delta}^+$  and  $\Omega_{\Delta}^{+,up}$ .

	full measurement		partial measurement	
	noiseless data	noisy data	noiseless data	noisy data
Noise in $I^0 f$	0%	5.4%	0%	6.8%
Noise in $I^1 f$	0%	4.0%	0%	3.3%
Error in $L^2(\Omega_{\Delta}^+)$	15.7%	20.5%	80.9%	77.4%
Error in $L^2(\Omega_{\Delta}^{+,up})$	15.5%	20.1%	59.8%	60.2%

As noted in Remark 1, the theoretical reconstruction applies to compactly supported vector fields. However, the numerical experiments consider two vectors fields with support touching the boundary. Yet, the algorithm applies due to the regularizing effect by the truncation in the Fourier series. For the same order of truncation, the difference in the reconstruction error of the original vector fields

supported up to the boundary and its corresponding one-layer-cutoff-away-from-the-boundary show no significant differences: contrast the two rows in the full measurement case in Tables 1 and 2.

The relative error in the reconstruction from partial data is commensurate to the error obtained by taking three derivatives: Specifically, numerical solutions of each of the discretized integral equations in Steps 5 and 8 amount to taking half a derivative of the noise (as shown in [8]), followed by taking two more derivatives in Step 10. Although the relative errors in reconstructions are significant, it is evident that the proposed method reasonably recovers the overall structure of the vector field, while conventional methods primarily focused on reconstructing the solenoidal component.

The neighborhoods  $\mathcal{N}_s$  can be chosen for each triangle (element-wise), and it might depend on the profile of the vector field, the distance from boundaries, and other discretization parameters. The optimal choice requires further quantitative studies since it depends on various factors. Errors in Experiment 2 are significantly larger than those in Experiment 1 in the partial measurement case. Further studies are also needed to clarify the relation of errors and phantom properties.

## 5. CONCLUSION

We present a first partial reconstruction result in the non-local vector tomography problem of recovering a planar vector field from its zero and first momenta ray transforms when data is only available on a strict subset of lines (the ones passing through an arc  $\Lambda$ ).

The reconstruction is based on solving an inverse boundary value problem for a system of Bukhgeim-Beltrami equations with partial data on a boundary arc  $\Lambda$ . The key step is transporting the data from  $\Lambda$  to the inner chord  $L$  (inaccessible by direct measurement) by solving an ill-posed Cauchy type singular integral equation.

The theoretical results in this paper extend to tensors of arbitrary order  $m \geq 2$ , where transportation of data from the boundary arc  $\Lambda$  to the inner chord  $L$  can be done at each of the sweep down steps in the method in [6]. However, at each of the  $(m + 1)$  steps, the reconstruction would require solving an unstable singular integral equation followed by taking a derivative. The increase in the order of ill-posedness with the order of the tensor renders the method difficult to apply for reconstruction of higher order tensors. The method still yields a unique determination result in this non-local problem.

## ACKNOWLEDGMENT

The work of H. Fujiwara was supported by JSPS KAKENHI Grant Numbers JP22K18674 and JP24K00539.

## REFERENCES

- [1] A. L. Bukhgeim, *Inversion Formulas in Inverse Problems*, chapter in *Linear Operators and Ill-Posed Problems* by M. M. Lavrentiev and L. Ya. Savalev, Plenum, New York, 1995.
- [2] A. Denisiuk, *Iterative inversion of the tensor momentum x-ray transform*, *Inverse Problems* **39** (10), (2023), 105002.
- [3] E. Derevtsov and I. Svetov, *Tomography of tensor fields in the plane*, *Eurasian J. Math. Comput. Appl.*, **3**(2) (2015), 24–68.
- [4] E. Derevtsov, Y. Volkov and T. Schuster, *Generalized attenuated ray transforms and their integral angular moments*, *Appl. Math. and Comput.*, **409** (2021), 125494.
- [5] E. Derevtsov, *Ray Transforms of the Moments of Planar Tensor Fields*, *J. Appl. Ind. Math.*, **17** (2023), 521–534.
- [6] H. Fujiwara, D. Omogbhe, K. Sadiq and A. Tamasan, *Inversion of the attenuated momenta ray transform of planar symmetric tensors*, *Inverse Problems* **40**(7) (2024), 33pp.
- [7] H. Fujiwara, K. Sadiq and A. Tamasan, *Numerical reconstruction of radiative sources in an absorbing and non-diffusing scattering medium in two dimensions*, *SIAM J. Imaging Sci.*, **13**(1) (2020), 535–555.
- [8] H. Fujiwara, K. Sadiq and A. Tamasan, *Partial inversion of the 2D attenuated X-ray transform with data on an arc*, *Inverse Probl. Imaging* **16**(1) (2022), 215–228.
- [9] H. Fujiwara, K. Sadiq and A. Tamasan, *Numerical reconstruction of radiative sources from partial boundary measurements*, *SIAM J. Imaging Sci.*, **16**(2) (2023), 948–968.
- [10] M. A. GOLBERG, *Introduction to the numerical solution of Cauchy singular integral equations*, in *Numerical solution of integral equations*, vol. 42 of *Math. Concepts Methods Sci. Engng.*, Plenum, New York, 1990, pp. 183–308.
- [11] S. Holman and P. Stefanov, *The weighted Doppler transform*, *Inverse Probl. Imaging*, **4** (2010), 111–130.
- [12] J. Ilmavirta and K. Mönkkönen, *Partial Data Problems and Unique Continuation in Scalar and Vector Field Tomography*, *J. Fourier Anal Appl* **28** (34) (2022).
- [13] N. I. IOAKIMIDIS, *A remark on singular integral equations with generalized kernels*, *SIAM J. Appl. Math.*, 44 (1984), pp. 1106–1111.

- [14] S. Jathar, M. Kar, V. Krishnan, and V. Sharafutdinov, *Normal Operators for Momentum Ray Transforms, I: The Inversion Formula*, *J Fourier Anal Appl* **30** (58) (2024).
- [15] S. G. Kazantsev and A. A. Bukhgeim, *Inversion of the scalar and vector attenuated X-ray transforms in a unit disc*, *J. Inverse Ill-Posed Probl.*, **15** (2007), 735–765.
- [16] F. W. King, *Hilbert Transforms*, Vol. 1, *Encyclopedia Math. Appl.*, **124**, Cambridge University Press, Cambridge, (2009)
- [17] W. Koppelman and J. D. Pincus, *Spectral representations for finite Hilbert transformations*, *Math. Z.*, **71** (1959), 399–407.
- [18] V. P. Krishnan, R. Manna, S. K. Sahoo, and V. A. Sharafutdinov, *Momentum ray transforms*, *Inverse Problems Imaging* **3** (13) (2019), 679–701.
- [19] V. P. Krishnan, R. Mishra and F. Monard *On solenoidal-injective and injective ray transforms of tensor fields on surfaces*, *J. Inverse Ill-Posed Problems* **27** (4) (2019), 527–538.
- [20] L. Kunyansky, E. McDugald, and B. Shearer, *Weighted Radon transforms of vector fields, with applications to magnetoacoustoelectric tomography*, *Inverse Problems* **39** (6) (2023), 065014.
- [21] M.M. Lavrentiev, *Some Improperly Posed Problems of Mathematical Physics*, New York: Springer, 1967.
- [22] A. Louis, *Inversion formulae for ray transforms in vector and tensor tomography*, *Inverse Problems* **38**:065008 (2022).
- [23] S. Maltseva, *An iterative method to solving the problem of reconstructing a 2-tensor field from limited data*, *Eurasian Journal of Mathematical and Computer Applications*, **10**(2), (2022) 42–54.
- [24] S. Maltseva, I. Svetov, A. Louis, *An iterative algorithm for reconstructing a 2D vector field by its limited-angle ray transform*, *Journal of Physics: Conference Series*, **1715**(1): 012037 (2021).
- [25] R. K. Mishra, *Full reconstruction of a vector field from restricted Doppler and first integral moment transforms in  $\mathbb{R}^n$* , *J. Inverse Ill-Posed Problems* **28** (2019), 173–184.
- [26] N. I. Muskhelishvili, *Singular Integral Equations*, Dover, New York, 2008.
- [27] G. P. Paternain, M. Salo, and G. Uhlmann, *Tensor Tomography: Progress and Challenges*, *Chin. Ann. Math. Ser. B.*, **35**(3) (2014), 399–428.
- [28] K. Sadiq and A. Tamasan, *On the range of the attenuated Radon transform in strictly convex sets*, *Trans. Amer. Math. Soc.*, **367**(8) (2015), 5375–5398.
- [29] K. Sadiq and A. Tamasan, *On the range characterization of the two dimensional attenuated Doppler transform*, *SIAM J. Math. Anal.*, **47**(3) (2015), 2001–2021.
- [30] K. Sadiq, A. Tamasan, *On the range of the X-ray transform of symmetric tensors compactly supported in the plane*, *Inverse Probl. Imaging* **17**(3) (2023), 660–685.
- [31] T. Schuster, *20 years of imaging in vector field tomography: a review*. In Y. Censor, M. Jiang, A.K. Louis (Eds.), *Mathematical Methods in Biomedical Imaging and Intensity-Modulated Radiation Therapy (IMRT)*, in: *Publications of the Scuola Normale Superiore*, CRM **7** (2008) 389–424.
- [32] V. A. Sharafutdinov, *Integral geometry of tensor fields*, VSP, Utrecht, 1994.
- [33] V. A. Sharafutdinov, *The Reshetnyak formula and Natterer stability estimates in tensor tomography*, *Inverse Problems*, **33** (2) (2017), 025002.
- [34] G. Sparr, K. Stråhlén, K. Lindström, and H. W. Persson, *Doppler tomography for vector fields*, *Inverse Problems*, **11** (1995), 1051–1061.
- [35] H. TAKAHASHI AND M. MORI, *Double exponential formulas for numerical integration*, *Pub. Res. Inst. Math. Sci.*, **9** (1974), pp. 721–741.
- [36] H. Widom, *Singular integral equations in  $L_p$* , *Trans. Amer. Math. Soc.*, **97** (1960), 131–160.

GRADUATE SCHOOL OF INFORMATICS, KYOTO UNIVERSITY, YOSHIDA HONMACHI, SAKYO-KU, KYOTO 606-8501, JAPAN  
*Email address:* fujiwara@acs.i.kyoto-u.ac.jp

JOHANN RADON INSTITUTE FOR COMPUTATIONAL AND APPLIED MATHEMATICS (RICAM), ALTENBERGERSTRASSE 69,  
 4040 LINZ, AUSTRIA  
*Email address:* kamran.sadiq@ricam.oeaw.ac.at

DEPARTMENT OF MATHEMATICS, UNIVERSITY OF CENTRAL FLORIDA, ORLANDO, 32816 FLORIDA, USA  
*Email address:* tamasan@math.ucf.edu